

# Exploring the Adversarial Frontier: Quantifying Robustness via Adversarial Hypervolume

Ping Guo, Cheng Gong, Xi Lin, Zhiyuan Yang, Qingfu Zhang  
Department of Computer Science, City University of Hong Kong, Hong Kong

**Abstract**—The escalating threat of adversarial attacks on deep learning models, particularly in security-critical fields, has underscored the need for robust deep learning systems. Conventional robustness evaluations have relied on adversarial accuracy, which measures a model’s performance under a specific perturbation intensity. However, this singular metric does not fully encapsulate the overall resilience of a model against varying degrees of perturbation. To address this gap, we propose a new metric termed adversarial hypervolume, assessing the robustness of deep learning models comprehensively over a range of perturbation intensities from a multi-objective optimization standpoint. This metric allows for an in-depth comparison of defense mechanisms and recognizes the trivial improvements in robustness afforded by less potent defensive strategies. Additionally, we adopt a novel training algorithm that enhances adversarial robustness uniformly across various perturbation intensities, in contrast to methods narrowly focused on optimizing adversarial accuracy. Our extensive empirical studies validate the effectiveness of the adversarial hypervolume metric, demonstrating its ability to reveal subtle differences in robustness that adversarial accuracy overlooks. This research contributes a new measure of robustness and establishes a standard for assessing and benchmarking the resilience of current and future defensive models against adversarial threats.

**Index Terms**—Adversarial Attacks, Multiobjective Optimization, Hypervolume

## I. INTRODUCTION

The increasing emphasis on evaluating the inherent robustness of deep learning (DL) models and developing more robust DL systems constitutes a pivotal area of research within the machine learning (ML) community [1]–[5]. This paradigm shift is primarily driven by growing security concerns associated with *adversarial attacks* on deep neural network-based (DNN) image classification systems. These attacks introduce imperceptible perturbations to input images, which are typically indistinguishable from the human eye, leading to incorrect classifications by the DNN model [6]–[8]. The potential implications of such vulnerabilities are particularly alarming in contexts critical to security, such as face recognition [9] and autonomous driving [10], where the consequences of misclassification could be severe. Nonetheless, efforts to construct adversarially robust models face substantial challenges, particularly the absence of a comprehensive evaluation framework for rigorously evaluating the robustness of DL models.

Conventionally, *adversarial accuracy* has been the principal metric for robustness evaluation, measuring a model’s resilience to adversarial examples generated through a range of attack strategies [7], [11], [12]. The emergence of increasingly sophisticated attacks, such as the Fast Gradient Sign Method (FGSM) [7], DeepFool [13], Projected Gradient Descent (PGD) [1], and Auto Projected Gradient Descent (APGD) [14], has led to an expansion of benchmark adversarial accuracies. Despite this, the field lacks a unified robustness metric due to the differing adversarial accuracy results across various attacks. Notably, the integration of APGD [14] and Square Attack [15] within AutoAttack [14] has established a widely recognized benchmark for adversarial accuracy assessment. The development of standard toolkits like RobustBench [16] has also substantially advanced the uniform comparison of adversarial defense capabilities across different defensive models, positioning the adversarial accuracy of the models under AutoAttack as the gold standard.

Recent research has challenged the adequacy of adversarial accuracy as the robustness metric for DL models, demonstrating that it fails to capture the full scope of a model’s resilience against attacks [11], [17], [18]. Robey *et al.* [17] have proposed the probability of misclassification as a more comprehensive measure of robustness, calculated through random sampling, although they acknowledge the computational challenges posed by the complexity of high-dimensional spaces. Oliver *et al.* [18] have explored non-adversarial spaces using geometric methods, assessing the extent of these regions within the sample space as an indicator of robustness. Despite these contributions, one can argue that neither misclassification probability nor adversarial region size sufficiently represent a model’s robustness, as they fail to consider the variation in a model’s response to varying levels of perturbation intensities.

To address the shortcomings of existing robustness metrics, which focus solely on model robustness at a fixed perturbation level, we introduce a new metric called *adversarial hypervolume*. This metric evaluates DL model robustness by examining the normalized confidence scores of worst-case adversarial examples across various levels of perturbation intensities. It facilitates meaningful comparisons between defensive models with comparable adversarial accuracy and evaluation of the incremental robustness improvements provided by weaker defensive measures like Feature Squeezing and JPEG compression [19]. A higher adversarial hypervolume metric value indicates improved model robustness throughout various perturbation intensities, thereby offering a more comprehensive

This paper was produced by the IEEE Publication Technology Group. They are in Piscataway, NJ.

Manuscript received April 19, 2021; revised August 16, 2021.

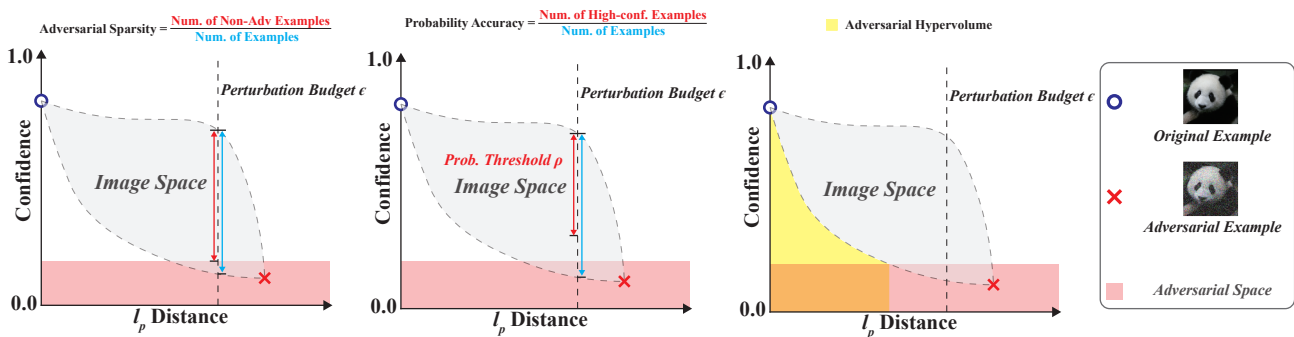


Fig. 1. **Comparison between adversarial hypervolume and established robustness metrics.** *Adversarial sparsity* measures the proportion of non-adversarial to total examples at perturbation level  $\epsilon$ . *Probability accuracy* denotes the ratio of high-confidence predictions to total examples at the perturbation level  $\epsilon$ . *Adversarial hypervolume* represents the averaged variations in confidence scores over a range of perturbation intensities.

assessment of a model’s resilience against adversarial attacks. We illustrate a conceptual comparison between our proposed metric and two existing metrics in Fig. 1.

Our metric, adversarial hypervolume, is based on the concept of hypervolume [20] from the multi-objective optimization literature [21]–[23]. We begin by constructing a multi-objective optimization problem that mirrors the complexity of actual attack scenarios, with the dual aims of minimizing the perturbation’s magnitude and simultaneously reducing the model’s confidence in the original classification. In contrast, much of existing research approaches the problem from the perspective of single-objective optimization with a distance constraint [1], [7] or employs a weighted sum of multiple objectives [11]. We subsequently delineate a set of adversarial examples that illustrate the model’s unique vulnerability landscape when subjected to an attack. Each example signifies a nadir of confidence corresponding to a particular magnitude of perturbation, thereby delineating the *adversarial frontier*. This concept is inspired by the Pareto optimality principle [21]. Ultimately, we quantify a model’s robustness by calculating the adversarial hypervolume, which measures the size of the region demarcated by the adversarial frontier.

In summary, our contributions are as follows:

- We introduce a novel metric, the adversarial hypervolume, which quantifies the robustness of DL models against a range of perturbation intensities, thus offering a comprehensive evaluation of a model’s resilience to adversarial attacks.
- Employing this metric, we propose a straightforward method for its computation and adopt an efficient training algorithm to enhance the robustness of DL models.
- Our empirical findings reveal that the adversarial hypervolume effectively measures the enhancement of robustness from weaker defensive mechanisms (*i.e.*, input transformations) and delivers important supplementary insights, such as average confidence variation, which serve as valuable adjuncts to adversarial accuracy.
- By conducting comprehensive experiments, we have assessed the robustness of cutting-edge state-of-the-art (SOTA) defensive models, thereby setting a benchmark for future studies.

## II. RELATED WORK

### A. Adversarial Attacks and Defenses

**Adversarial Attacks.** Since the discovery of adversarial vulnerabilities in DL models [6], a substantial body of research has focused on the development of attack algorithms within various threat models to critically evaluate the robustness of these models [24]–[26]. Specifically, researchers have developed *white-box* attacks by leveraging complete access to a model’s parameters and gradients; in contrast, *black-box* attacks are devised with merely an understanding of the model’s input-output interface available to the attacker.

*White-box Attacks.* Exploiting full knowledge of the model, including its gradients, white-box attacks evaluate a model’s robustness by formulating and solving an optimization problem [1]. This practice has led to the development of a series of attacks, including the PGD attack [1], the Carlini-Wagner (CW) attack [11], the FGSM attack [7], the Basic Iterative Method (BIM) attack [8], and the DeepFool attack [13]. A model’s adversarial accuracy, when subjected to these attacks, is a critical metric for determining its robustness.

*Black-box Attacks.* Despite the efficacy of white-box attacks in assessing robustness, their real-world applicability is often restricted due to limited access to internal model details. Therefore, many black-box attacks have been developed to overcome this limitation [27]–[32]. Among them, the Square attack stands out, successfully breaching the SOTA defenses using a gradient-free strategy and even surpassing some gradient-based attacks that have access to comprehensive information [14]. Within the AutoAttack framework [14], it is a critical component, utilized alongside the APGD attack to measure a model’s adversarial accuracy.

**Adversarial Defenses.** Defensive strategies against adversarial attacks are designed to enhance a model’s inherent robustness or alleviate the effects of adversarial attacks. To improve the robustness, a range of adversarial training techniques have been introduced [1], [33]. Furthermore, several tactics have been devised to detect or neutralize adversarial examples, including input transformation [19], [34], adversarial purification [35], [36], and stateful defenses [37], [38]. Given that adversarial purification and stateful defenses are tailored

for real-world classification systems rather than a standalone model, our study concentrates primarily on the robustness improvement brought by adversarial training and input transformation techniques.

**Adversarial Training.** Adversarial training represents a prevalent approach to increase the robustness of DL models by incorporating adversarial examples into the training dataset, which enables the model to learn more robust decision boundaries [1]. Adversarial examples are often generated using the PGD attack [1], and a significant volume of research corroborates its efficacy [39]–[41].

**Input transformation.** Input transformation is a cost-effective defensive strategy that can be seamlessly incorporated into systems with adversarially trained models to enhance robustness [19], [34]. However, the efficacy of input transformation has come into question, as it has been proven to be vulnerable to circumvention [12]. Moreover, using adversarial accuracy to measure the robustness improvement from input transformation techniques may lead to misleading results, since the adversarial accuracy of disparate techniques tends to be low and indistinguishable. In contrast, our research introduces the adversarial hypervolume metric, which facilitates a comparative analysis of robustness improvements by providing more detailed insights into average confidence values.

### B. Alternative Metrics for Evaluating Robustness

Although adversarial accuracy is commonly used as a primary metric to assess model robustness, researchers have proposed several alternative measures to offer a more comprehensive understanding of model robustness. These include the minimum adversarial perturbation [11], probabilistic robustness [17], and adversarial sparsity [18].

**Minimal Perturbation.** Measuring the smallest perturbation magnitude required to alter an input into an adversarial example is a prevalent method for evaluating the robustness of a model. Carlini *et al.* addressed this through an optimization problem that balances the perturbation size and the confidence of the adversarial example by considering their linear combination [11]. However, this metric fails to fully capture the spectrum of a model’s robustness (confidence score) across various perturbation levels.

**Probabilistic robustness.** Robey *et al.* introduced a metric to assess probabilistic robustness, shifting the focus from the conventional *worst-case* scenario [17]. Rather than just considering the adversarial accuracy, this metric evaluates the likelihood of a model’s correct predictions in the presence of adversarial perturbations. The downside is its computational intensity, often necessitating Monte Carlo simulations to approximate the adversarial example distribution, especially in high-dimensional spaces.

**Adversarial Sparsity.** Recent research by Oliver *et al.* has presented the concept of adversarial sparsity, which probes the boundary of non-adversarial regions to determine their proportion within the entire sample space [18]. Although the method aligns with the principles of probabilistic robustness,

Oliver *et al.* suggest a geometric method to determine the adversarial sparsity, which yields improved convergence results. Despite these advancements, measuring this metric remains challenging in high-dimensional spaces.

## III. ADVERSARIAL HYPERVOLUME

This section introduces the concept of adversarial hypervolume, a novel metric developed to assess the robustness of DL models against adversarial attacks. Initially, we outline the multi-objective optimization problem foundational to the adversarial hypervolume concept in Section III-A. Subsequently, we describe the adversarial frontier in Section III-B and detail the methodology for computing the adversarial hypervolume in Section III-C. We then explore the relationship between adversarial hypervolume, adversarial accuracy, and other established metrics in Section III-D.

### A. Multiobjective Adversarial Problem

Consider a classifier  $f : \mathcal{X} \rightarrow \mathcal{Y}$ , where  $\mathcal{X} \subseteq [0, 1]^d$  represents the input image space, and  $\mathcal{Y} \subseteq [0, 1]^m$  corresponds to the output space implicating a probability distribution across  $m$  class labels. The aim of the adversarial attack is to determine the perturbation  $\delta$  for a given unperturbed data point  $(x, y)$  as expressed in:

$$\min_{\delta} \mathcal{L}(f, x, y, \delta) = (\mathcal{L}_{\text{conf}}(f, x, y, \delta), \mathcal{L}_{\text{dist}}(\delta)). \quad (1)$$

In this formula,  $\mathcal{L}_{\text{conf}}$  denotes the confidence loss, while  $\mathcal{L}_{\text{dist}}$  indicates the distance loss. Cutting-edge attacks typically utilize the negative cross-entropy loss to measure confidence loss and the  $\ell_p$  norm distance to quantify distance loss. These attacks typically focus on minimizing an aggregated loss function or optimizing the confidence loss subject to a constraint on the distance loss [1], [11].

**Motivation.** The conventional approach for creating adversarial examples typically limits the secondary objective (*e.g.*,  $\|\delta\| \leq \epsilon$ ), focusing exclusively on optimizing the primary objective [1], [11]. However, this strategy does not thoroughly explore the loss landscape, thus failing to comprehensively evaluate the model’s robustness. Our study introduces the use of the hypervolume indicator as a comprehensive metric to assess the robustness of the model by measuring the set of optimal trade-offs between the two objectives.

### B. Adversarial Frontier

Drawing on the multiobjective adversarial framework outlined in Section III-A, we incorporate the multiobjective optimization principles to pinpoint optimal trade-off solutions. We begin by elucidating the concepts of Pareto dominance and Pareto optimality, which are central to multi-objective optimization and represent the most efficient trade-off solutions. Subsequently, we employ an example to demonstrate the adversarial frontier delineated by these principles and to showcase the adversarial frontiers of various defensive models.

**Pareto dominance.** Consider two candidate perturbations  $\delta^a$  and  $\delta^b$ .  $\delta^a$  is said to *dominate*  $\delta^b$  if and only if, for all criteria

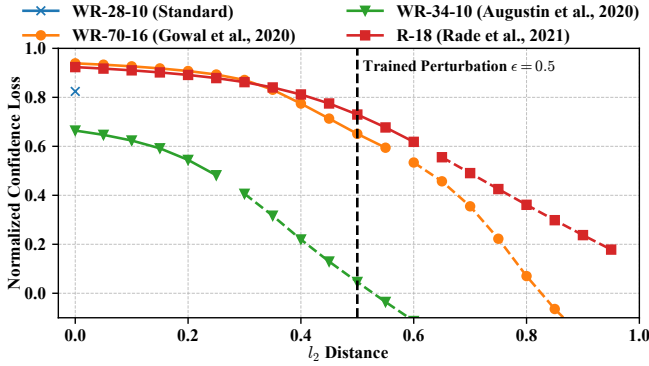


Fig. 2. The adversarial frontiers of different models computed using a randomly selected image from CIFAR-10 test set. R is for ResNet and WR is for WideResNet. The solid line means the example is correctly classified, the dashed line means the example is misclassified.

$i$  within the set  $\{\text{conf}, \text{dist}\}$ ,  $\mathcal{L}_i(\delta^a)$  is less than or equal to  $\mathcal{L}_i(\delta^b)$ , and there exists at least one criterion  $j$  for which  $\mathcal{L}_j(\delta^a)$  is strictly less than  $\mathcal{L}_j(\delta^b)$ .

**Pareto optimal.** A perturbation  $\delta^*$  is said to be *Pareto optimal* if and only if there is no alternative perturbation  $\delta$  exists that dominates  $\delta^*$ . The set of all such Pareto optimal perturbations constitutes the *Pareto set* in the sample space and the *Pareto front* in the loss space. Within the specific context of adversarial attacks, this ensemble is termed the *adversarial frontier*.

To give an intuitive understanding of the adversarial frontier, we first implement the confidence loss and distance loss and then visualize the adversarial frontiers of several defensive models. Specifically, we employ the  $\ell_2$  norm as the metric for distance loss, owing to its widespread acceptance and inherent simplicity. Subsequently, we implement the confidence loss in the following form:

$$\mathcal{L}_{\text{CE-conf}}(f, x, y, \delta) = \begin{cases} \text{CE}_{\text{norm}} & \text{if } \text{CE}_{\text{norm}} > 0 \\ 0 & \text{otherwise} \end{cases}, \quad (2)$$

$$\text{CE}_{\text{norm}}(f, x, y, \delta) = \frac{\log m + \log f_y(x + \delta)}{\log m}.$$

This expression denotes the normalized cross-entropy loss, selected for its characteristic whereby a negative value definitively signifies an instance misclassified by the model. A detailed discussion of this attribute is provided in Section VI-A.

Upon resolving the optimization problem in Equation (1), we obtain the adversarial frontiers corresponding to various models<sup>1</sup>. Specifically, we examine three adversarially trained models on the CIFAR-10 dataset [42]: ResNet-18 (R-18) [43], WideResNet-70-16 (WR-70-16) [41], and WideResNet-34-10 (WR-34-10) [44], all sourced from the RobustBench repository [16]. Each model has been trained with an  $\ell_2$  perturbation budget of  $\epsilon = 0.5$ . For contrastive analysis, we incorporate a standardly trained WideResNet-28-10 model. We plot the

<sup>1</sup>Here, we simply optimize the confidence loss using established attacks (PGD) with multiple fixed perturbations to derive these solutions, which is considered a basic approach to addressing the multiobjective problem (point-by-point).

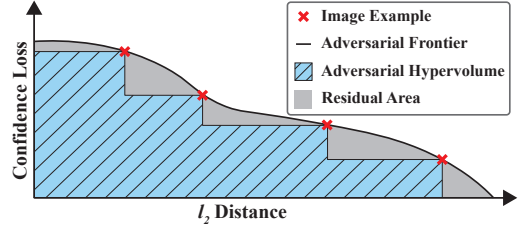


Fig. 3. An illustration of the adversarial hypervolume. Intuitively, it functions as an approximation of the integral of confidence values, where the gray area represents the approximation's residual error.

adversarial frontiers of these models using a randomly selected image from the test set in Fig. 2.

Fig. 2 illustrates that the normalized confidence loss of the standardly trained model decreases significantly with minimal perturbation, in contrast with the adversarially trained counterparts that preserve the confidence level within a small perturbation margin. Nonetheless, it is challenging to compare the robustness of models such as R-18 and WR-70-16 with reference to the adversarial frontiers derived from a singular image. To address this, we introduce the adversarial hypervolume indicator, a new metric designed to quantify the robustness of models uniformly across different perturbation levels.

### C. Adversarial Hypervolume

We introduce the concept of adversarial hypervolume as an approximate of the integral over the adversarial frontier. Consider a set  $\Delta$  consisting of  $K$  points  $\Delta = \{\delta_0, \dots, \delta_K\}$ , where each  $\delta_i$  satisfies  $\delta_i < \epsilon$ . The hypervolume indicator is computed as follows:

$$HV(\Delta, \mathbf{r}) = \Lambda\left(\bigcup_{\delta \in \Delta} \{z \in \mathbb{R}^m \mid \mathbf{r} \preceq z \preceq \delta\}\right). \quad (3)$$

Here  $\mathbf{r} \in \mathbb{R}^m$  represents the reference point,  $\Lambda$  represents the Lebesgue measure defined as  $\Lambda(Z) = \int_{z \in Z} \mathbb{1}_Z(z) dz$ , and  $\mathbb{1}_Z$  is the indicator function that is 1 if  $z \in Z$  and 0 otherwise. For our purposes, the reference point is set at  $(0, 0)$ , and  $m$  equals two, reflecting the consideration of two objectives. Fig. 3 provides an illustration of the adversarial hypervolume.

### D. Adversarial Hypervolume and Adversarial Accuracy

In this section, we demonstrate that our proposed adversarial hypervolume metric delivers more granular insights than adversarial accuracy. Drawing on a multiobjective framework, we propose the adversarial frontier curve concept, and we clarify the association between the adversarial hypervolume and the area under the curve. Furthermore, our analysis examines the interconnections among the adversarial hypervolume metric, adversarial accuracy, and adversarial sparsity.

**Marginal Confidence Loss.** Within our multiobjective adversarial framework, we can implement a variety of confidence loss functions. We have chosen to utilize the marginal confidence loss to examine the correlation between our proposed

metric and adversarial accuracy in this section. The marginal confidence loss is mathematically expressed as:

$$\begin{aligned} \mathcal{L}_{\text{MAR\_conf}}(f, x, y, \delta) &= \begin{cases} \text{MAR} & \text{if MAR} > 0 \\ 0 & \text{otherwise} \end{cases} \\ \text{MAR}(f, x, y, \delta) &= f_y(x + \delta) - \max_{i \neq y} f_i(x + \delta) \end{aligned} \quad (4)$$

Compared to normalized cross-entropy loss  $\text{CE}_{\text{norm}}$ , the marginal confidence loss demonstrates increased sensitivity to errors in classification. A negative MAR indicates a model's misclassification, satisfying both the necessary and sufficient conditions for a classification error.

**Adversarial Frontier Curve.** Addressing the optimization challenge delineated by Equation (1), we derive the adversarial frontiers corresponding to various models. These frontiers are represented as a parameterized curve, denoted as  $F(z)$ , where  $z$  indicates the perturbation magnitude. The curve characterizes the minimum  $\mathcal{L}_{\text{MAR\_conf}}$  at each perturbation level:

$$F(z) = \min_{\delta} \mathcal{L}_{\text{MAR\_conf}}(f, x, y, \delta), \quad \text{s.t. } \|\delta\| = z. \quad (5)$$

**Adversarial Hypervolume.** The adversarial hypervolume, denoted by  $\text{AH}_{\text{MAR}}(f, x, y, \epsilon)$ , where  $\epsilon$  represents the perturbation budget, is calculated by integrating the adversarial frontier curve across the full spectrum of possible perturbations. The relationship is formally expressed as follows:

$$\text{AH}_{\text{MAR}}(f, x, y, \epsilon) = \int_0^{\epsilon} F(z) dz - \mathbf{e}, \quad (6)$$

where  $\mathbf{e}$  denotes the error term that quantifies the discrepancy between the integral and the computed adversarial hypervolume. Furthermore, we provide a convergence analysis of the error term  $\mathbf{e}$  in Section III-E.

**Adversarial Accuracy.** To establish the relationship between adversarial accuracy and adversarial hypervolume, we first specify the expression for adversarial accuracy at a specific perturbation level  $z$  using the sign function:

$$\text{AA}(f, x, y, z) = \text{sign}_+(F(z)). \quad (7)$$

Subsequently, we define the average adversarial accuracy across the entire range of perturbations as:

$$\overline{\text{AA}}(x, y, \epsilon) = \int_0^{\epsilon} \text{sign}_+(F(z)) dz. \quad (8)$$

It is evident that by employing the marginal loss as a confidence proxy, the adversarial hypervolume encompasses a broader array of information than adversarial accuracy alone. Moreover, another implementation using the normalized confidence loss enhances this metric by integrating the insights gained from misclassified examples, rendering it a more comprehensive and robust measure of model resilience.

**Adversarial Sparsity.** Since the adversarial sparsity [18] quantifies the extent of the misclassified region within the entire sample space, adversarial accuracy at a given perturbation level  $z$  can be expressed as:

$$\text{AA}(f, x, y, z) = 1 - \text{sign}_+(1 - \text{AS}(f, x, y, z)) \quad (9)$$

The integration of adversarial accuracy over the complete range of perturbations is represented by:

$$\overline{\text{AA}}(f, x, y, \epsilon) = \int_0^{\epsilon} 1 - \text{sign}_+(1 - \text{AS}(f, x, y, z)) dz \quad (10)$$

**Connection and Difference.** Our metric emphasizes correctly classified instances, in contrast to adversarial sparsity, which focuses on the analysis of misclassified samples. Consequently, it constitutes an important complement for assessing a model's robustness. Moreover, our metric captures the average effect across the perturbation space, diverging from adversarial sparsity that is confined to a specific perturbation distance. This difference is rooted in the need for computational viability: the calculation of adversarial sparsity over a comprehensive perturbation range is impractical due to its prohibitive computational demand. Conversely, our metric design emphasizes computational efficiency, enabling its application to large-scale datasets.

### E. Approximation Error

This section presents a convergence analysis of the approximation error term  $\mathbf{e}$  for the adversarial hypervolume in relation to the integral of the adversarial frontier.

For an image  $(x, y)$ , a classifier  $f$ , its corresponding adversarial frontier as  $\mathcal{L}_{\text{conf}} = F(z)$ , where  $z$  is the magnitude of the perturbation, usually measured by the  $p$ -norm. It must be a monotonic non-increasing function by definition of the adversarial front. Moreover, we assume that the following conditions hold:

**Assumption 1.**  $F(z)$  is Lipschitz-continuous, i.e.,  $\exists L_0 > 0, \forall z_1, z_2, |F(z_1) - F(z_2)| \leq L_0 |z_1 - z_2|$ .

When approximating the integral of the adversarial frontier over the interval  $[0, \epsilon]$  using  $N$  points  $\{0, \frac{\epsilon}{N}, \frac{2\epsilon}{N}, \dots, \frac{\epsilon}{N}\}$ , let us consider the error  $\mathbf{e}_i$  within each subinterval  $[\frac{i\epsilon}{N}, \frac{(i+1)\epsilon}{N}]$ :

$$\begin{aligned} \mathbf{e}_i &= \int_{\frac{i\epsilon}{N}}^{\frac{(i+1)\epsilon}{N}} F(z) dz - F\left(\frac{(i+1)\epsilon}{N}\right) \frac{\epsilon}{N} \\ &= \int_{\frac{i\epsilon}{N}}^{\frac{(i+1)\epsilon}{N}} F(z) - F\left(\frac{(i+1)\epsilon}{N}\right) dz \\ &\leq \int_{\frac{i\epsilon}{N}}^{\frac{(i+1)\epsilon}{N}} L_0 \left(z - \frac{(i+1)\epsilon}{N}\right) dz \\ &= \frac{\epsilon^2}{N^2} L_0 \end{aligned} \quad (11)$$

where  $\mathbf{e}_i$  is the error for a given subinterval. Summation of errors across all  $N$  subintervals yields the total approximation error  $\mathbf{e}$ , which can be expressed as follows:

$$\mathbf{e} = N \mathbf{e}_i \leq \frac{\epsilon^2}{N} L_0 \quad (12)$$

## IV. ALGORITHM

This section delineates algorithms designed to identify adversarial frontiers and compute adversarial hypervolume, in addition to proposing an adversarial training approach

---

**Algorithm 1** Adversarial Hypervolume Computation

---

**Input:** Data point  $(x, y)$ , perturbation budget  $\epsilon$ , model  $f$ , evaluation points  $N$   
**Output:** Adversarial Hypervolume AH  
 $AF = \emptyset$   
**for**  $i = 1$  **to**  $N$  **do**  
     $\delta = \text{PGD}(f, x, y, \frac{\epsilon}{N})$   
    **if**  $\mathcal{L}_{\text{conf}}(f, x, y, \delta) > 0$  **then**  
         $AF = AF \cup \{(\frac{i}{N}, 0)\}$   
        **break**  
    **else**  
         $AF = AF \cup \{(\frac{i}{N}, \mathcal{L}_{\text{conf}}(f, x, y, \delta))\}$   
    **end if**  
**end for**  
**return**  $AH = \text{Compute\_HV}(AF)$

---

that seeks to augment model robustness over a range of perturbation levels. Furthermore, this section elucidates the implementation details and analyzes the complexity inherent in these algorithms.

*A. Adversarial Hypervolume Computation*

The computation of adversarial hypervolume involves two primary steps: 1) identifying the adversarial frontier and 2) calculating the hypervolume of this frontier. Specifically, identification of the adversarial frontier necessitates employing strong attacks to discover a sequence of instances with the lowest possible confidence score across different levels of perturbation. Subsequently, the adversarial hypervolume is computed using methodologies from the field of multiobjective optimization.

**Identifying the Adversarial Frontier.** The detailed algorithm to calculate adversarial hypervolume is presented in Algorithm 1, centering on the identification of the examples that constitute the frontier. With a fixed perturbation budget of  $\epsilon$  and an intent to depict the adversarial frontier using  $N$  examples, we employ a strong attack method, such as the PGD attack, with perturbations  $\{0, \frac{\epsilon}{N}, \dots, \epsilon\}$ . This approach results in a set of examples, each characterized by the lowest confidence score at the respective perturbation level. Notably, examples with negative normalized scores are excluded since they represent misclassified examples, which could distort the model’s average robustness assessment.

**Calculating the Hypervolume.** To accurately calculate the hypervolume enclosed by the adversarial frontier, established algorithms from multiobjective optimization literature are employed. Specifically, in the case of a two-objective problem, the adversarial frontier is first organized in ascending order according to the perturbation level values. Subsequently, the volume within each interval  $[\frac{i\epsilon}{N}, \frac{(i+1)\epsilon}{N}]$  is determined by calculating the product of the interval’s length and the maximum objective value at the end of the interval, as shown in Figure 3.

**Batched Adversarial Hypervolume.** Implementing batch processing significantly enhances the computational efficiency

---

**Algorithm 2** Compute\_HV

---

**Input:** Adversarial Front AF  
**Output:** Adversarial Hypervolume AH  
 $AH = 0$   
 $AF = \text{Sort}(AF)$   
**for**  $i = 1$  **to**  $|AF|$  **do**  
     $AH = AH + (AF[i].x - AF[i - 1].x) \times AF[i].y$   
**end for**  
**return**  $AH$

---

of neural networks. In particular, the PGD algorithm can simultaneously process multiple images from the dataset concurrently, which does not impact the optimal solutions since the aggregate of their loss values does not affect the back-propagation process. Subsequent operations, such as sorting and hypervolume calculation for each image, can be efficiently executed in parallel using multithreading on the CPU, obviating the need for GPU interaction.

*B. Adversarial Hypervolume Training*

In the context of adversarial hypervolume training, our algorithm harnesses examples from the adversarial frontier to enhance the training process of DL model. The adopted training algorithm unfolds as follows:

- **Base Training Framework:** Our adopted training framework integrates the TRADES framework [39], augmented by Adversarial Weight Perturbation (AWP) [45], to serve as the cornerstone of our methodology. Employing this framework, along with a perturbation level, enables the generation of adversarial examples that augment the training process.
- **Ascending Perturbation Levels:** By progressively elevating the perturbation levels, we replicate adversarial examples stemming from the identified adversarial frontier, in accordance with the aforementioned algorithm. This method has demonstrated efficacy in enhancing model robustness and offers greater stability than conventional adversarial training approaches [46].

*C. Convergence and Complexity*

The convergence of the adversarial hypervolume computation algorithm primarily hinges on the precise identification of the adversarial frontier. Despite the challenges posed by the multiobjective nature of the problem when attempting to verify algorithmic convergence, such convergence can be substantiated by examining the optimality characteristics inherent in the PGD algorithm. We introduce the following assumption:

**Assumption 2.** *The PGD algorithm can identify the optimal solutions with the minimal confidence loss across various perturbation budgets [1].*

Under this assumption, no solutions can have an identical perturbation level, denoted as  $\delta$ , while presenting a lower confidence score. This implies that no solutions can dominate those found by the PGD algorithm. Consequently, the algorithm is assured to converge to the adversarial frontier.

TABLE I  
ADVERSARIAL HYPERVOLUME, ALONG WITH ADVERSARIAL ACCURACY OF DEFENSIVE MODELS UNDER MODIFIED AUTOATTACK [14] ON THE CIFAR-10 DATASET. THE CONFIDENCE LOSS IS THE NORMALIZED CROSS-ENTROPY LOSS MENTIONED IN EQUATION (2).

Model	Defense	$\ell_2$ Attack		$\ell_\infty$ Attack	
		Acc. (Std./Adv.)	AH (mean <sub>std</sub> )	Acc. (Std./Adv.)	AH (mean <sub>std</sub> )
WideResNet-28-10	None	94.78/02.58	0.2127 <sub>0.2191</sub>	94.78/01.65	0.0912 <sub>0.1905</sub>
ResNet-18	Madry <i>et al.</i> (2018) [1]	80.75/72.79	0.7269 <sub>0.3443</sub>	82.59/19.24	0.4758 <sub>0.3353</sub>
WideResNet-28-10	Wang <i>et al.</i> (2023) [40]	95.16/86.66	0.8273 <sub>0.1777</sub>	92.44/72.35	0.7019 <sub>0.2230</sub>
WideResNet-28-10	Rebuffi <i>et al.</i> (2021) [47]	91.79/83.31	0.8115 <sub>0.2004</sub>	87.33/67.91	0.6809 <sub>0.2434</sub>
WideResNet-70-16	Rebuffi <i>et al.</i> (2021) [47]	92.41/84.80	0.8309 <sub>0.1956</sub>	88.54/70.97	0.7113 <sub>0.2414</sub>
WideResNet-70-16	Rebuffi <i>et al.</i> (2021) [47] (w/ data)	95.74/85.18	0.8683 <sub>0.1760</sub>	92.23/71.84	0.7509 <sub>0.2347</sub>
ResNet-18	Sehwag <i>et al.</i> (2022) [48]	89.76/80.05	0.8378 <sub>0.2260</sub>	84.59/64.23	0.7075 <sub>0.2630</sub>
WideResNet-34-10	Sehwag <i>et al.</i> (2022) [48]	90.93/77.24	0.8556 <sub>0.2150</sub>	86.68/60.27	0.7502 <sub>0.2602</sub>
ResNet-18	Rade <i>et al.</i> (2022) [49]	90.57/81.27	0.8126 <sub>0.2154</sub>	86.86/64.81	0.6747 <sub>0.2399</sub>
ResNet-50	Augustin <i>et al.</i> (2020) [44]	91.08/78.81	0.7291 <sub>0.2802</sub>	-	-
WideResNet-34-10	Augustin <i>et al.</i> (2020) [44]	92.23/81.03	0.7534 <sub>0.2626</sub>	-	-
WideResNet-34-10	Huang <i>et al.</i> (2021) [50]	-	-	90.56/67.80	0.7437 <sub>0.2514</sub>
WideResNet-34-10	Huang <i>et al.</i> (2021) [50] (EMA)	-	-	91.23/68.54	0.7449 <sub>0.2467</sub>
WideResNet-28-10	<b>Ours</b>	91.43/88.57	0.7642 <sub>0.2053</sub>	88.87/63.62	0.6213 <sub>0.2270</sub>

## V. EVALUATION

### A. Experimental Setup

**Datasets and Classification Models.** To evaluate adversarial robustness comprehensively, we calculate the adversarial hypervolume of models equipped with various defensive strategies and adversarial training techniques. We focus on the CIFAR-10 dataset [42], consisting of 50,000 training images and 10,000 testing images, each with dimensions of  $32 \times 32$  pixels in full color, across ten distinct categories. This dataset is recognized as a pivotal benchmark for adversarial robustness evaluation. We utilize models from RobustBench [16], which encompasses both standardly and adversarially trained architectures. Moreover, we apply standardly trained models to evaluate input transformation defense techniques.

**Attack for Evaluation.** To carry out the evaluation, we employed a modified version of the AutoAttack algorithm [14]. This original algorithm comprises three different attacks: APGD-CE, APGD-DLR, and Square Attack. For our purposes, we incorporated only the first two attacks—APGD-CE and APGD-DLR—since the inclusion of the third attack does not significantly affect the outcome and a gradient-based approach is much faster than black-box approaches. Unless otherwise indicated, we standardized the attack parameters, setting the number of steps at 50 and the maximum perturbation magnitude at  $8/255$  for the  $\ell_\infty$  attack and 2.5 for the  $\ell_2$  attack, in order to calculate adversarial accuracy. Furthermore, the perturbation magnitude was divided into 10 equal intervals to facilitate the computation of the adversarial hypervolume.

**Defense Methods.** We consider measuring the robustness of the models under both methods to improve the inherent robustness (adversarial training) and methods to protect the input of the model (input transformation).

*Adversarial Training.* Adversarial training enhances the model robustness by utilizing augmented data samples crafted using various attack strategies. In this work, we use pre-trained

adversarially trained models using SOTA training methods, including [1], [40], [44], [47]–[50]. These models rank highly on the RobustBench leaderboard [16] and are widely used as strong robust baselines.

*Input Transformation.* Input transformations are straightforward defensive mechanisms that can be easily integrated into systems with adversarially trained models, contributing to an improvement in overall robustness. Our research reexamines several of these techniques, JPEG compression [34], Feature Squeezing, and Spatial Smoothing [19]. Notably, they are known to be weak and breakable defenses [12] and adversarial accuracy may not be adequate for comparing their efficacy.

### B. Results on Adversarially Trained Models

The adversarial hypervolumes and adversarial accuracies on current SOTA defensive models are shown in TABLE I. As adversarial hypervolume is a new metric that contains richer information than adversarial accuracy, it is overall consistent with the adversarial accuracy. Furthermore, all adversarially trained models demonstrate significantly greater adversarial hypervolumes compared to the undefended model, suggesting that adversarial training substantially enhances model robustness. The adversarial hypervolumes for defended models exceed 0.7 for  $\ell_2$  Attack and 0.6 for  $\ell_\infty$  Attack, in contrast to the undefended model’s markedly lower values of 0.2127 and 0.0912, respectively.

**Mismatch.** An inconsistency is observed among robust models, with a higher adversarial accuracy paired with a lower adversarial hypervolume. This discrepancy suggests a reduced average confidence across perturbation space for stronger models, attributable to two factors:

- a tendency to prioritize easy-to-recognize samples, resulting in lower confidence scores for more challenging ones, and thus a reduction in mean adversarial hypervolume.
- a generally lower confidence throughout the perturbation space, which may be indicative of an inherently conser-

TABLE II  
ABLATION STUDY FOR OUR TRAINING ALGORITHM UNDER CIFAR-10 DATASET.

Model	Defense	$\ell_2$ Attack		$\ell_\infty$ Attack	
		Acc. (Std./Adv.)	AH (mean <sub>std</sub> )	Acc. (Std./Adv.)	AH (mean <sub>std</sub> )
WideResNet-28-10	<b>Ours</b>	91.43/88.57	0.7642 <sub>0.2057</sub>	88.87/63.62	0.6213 <sub>0.2270</sub>
WideResNet-28-10	w./o. ascending	91.48/87.49	0.7563 <sub>0.2053</sub>	88.14/62.53	0.6209 <sub>0.2289</sub>
WideResNet-28-10	w./o. data	90.47/85.22	0.7447 <sub>0.2294</sub>	88.17/61.53	0.6377 <sub>0.2529</sub>

vative and less assured predictive capability, potentially signifying enhanced robustness.

**Dominance of Diffusion-based Defenses.** Notwithstanding the aforementioned incongruities, diffusion-based defensive mechanisms stand apart by achieving high measures in both adversarial accuracy and adversarial hypervolume. These methods facilitate model training by harnessing synthetic examples generated by diffusion models, which are trained to learn the data distribution. Specifically, models trained following the methodology of Rebuffi *et al.* [47] exhibit substantial improvements in adversarial hypervolume when exposed to synthetic data. Moreover, the SOTA adversarial accuracy recorded for our training approach also incorporated synthetic examples. Subsequent ablation studies were conducted to authenticate the contribution of synthetic examples to the enhanced adversarial hypervolume.

### C. Results on Adversarial Hypervolume Training

The efficacy of our adversarial hypervolume training techniques was investigated through an ablation study. The study involved two modifications:

- **Without Ascending.** We remove the ascending training strategy from the adversarial hypervolume training method and use the fixed perturbation strategy as done in most adversarial training methods.
- **Without Synthetic data.** We remove the synthetic data generated by the diffusion model and only use the original data for training.

**Results.** The findings, as presented in Table II, indicate that the standard approach outperforms alternative strategies concerning adversarial robustness, achieving the highest performance in adversarial accuracy and adversarial hypervolume during both  $\ell_2$  and  $\ell_\infty$  attacks, with the slight expense of clean accuracy. Elimination of the ascending gradient technique resulted in a marginal reduction in robustness metrics, confirming the trend of decreased stability documented in [46]. The absence of synthetic data not only impairs adversarial accuracy and hypervolume, but also leads to a reduction in the mean hypervolume alongside increased variability. These observations underscore the synthetic data’s role in bolstering defense mechanisms across a broad spectrum of samples, thus facilitating a more consistent model performance throughout the sample space.

### D. Results on Input Transformation

Input transformation techniques, while recognized as vulnerable and easily circumvented defenses, can be conveniently

TABLE III  
RESULTS ON INPUT TRANSFORMATION DEFENSE METHODS.

Trans. Methods	Acc. (Std./ $\ell_2$ Adv./ $\ell_\infty$ Adv.)	AH ( $\ell_2$ )	AH ( $\ell_\infty$ )
None	94.78/02.50/01.39	0.0009 <sub>0.0256</sub>	0.0000 <sub>0.0000</sub>
JPEG [34]	91.28/07.61/03.19	0.0521 <sub>0.2047</sub>	0.0001 <sub>0.0098</sub>
FS [19]	94.24/03.28/01.61	0.0418 <sub>0.1989</sub>	0.0394 <sub>0.1945</sub>
SPS [19]	87.33/20.21/05.91	0.2033 <sub>0.3765</sub>	0.0105 <sub>0.0929</sub>

integrated into systems to marginally enhance robustness. Despite its simplicity, evaluation of performance under the metric of adversarial accuracy presents challenges in making meaningful comparisons and deriving insights. Therefore, we employed the metric of adversarial hypervolume in our experimental assessment of the robustness of these methods.

**Results.** Table III presents the results for the various input transformation methods. All methods display significantly lower adversarial accuracies under both attack types. Furthermore, when employing prevalent perturbation budgets, the  $\ell_\infty$  attack is observed to be more potent than the  $\ell_2$  attack, as evidenced by the lower adversarial accuracy and hypervolume. Of all the input transformation methods evaluated, only spatial smoothing imparts some resistance to  $\ell_2$  attack, whereas none effectively withstand  $\ell_\infty$  attack. The adversarial hypervolume metric suggests that while these transformations can resist minor noise, they are ineffective against substantial perturbations.

### E. Convergence Results

**Analysis Settings.** We employ an adversarially trained model [1] to demonstrate the convergence properties of our algorithm in calculating the adversarial hypervolume. For these computations, we fixed  $N = 20$  as the upper bound for the number of points considered, and we approximated the true integral of the confidence score using these computed values. To derive the theoretical error function, we formulate and solve an optimization problem that minimizes the squared loss between the theoretically predicted loss (as specified in Equation (12)) and the observed error measurements, with  $L_0$  treated as a variable via CVXPY [51]. In additional configurations, we adopted the  $\ell_2$  norm for distance loss and the normalized cross-entropy loss for the confidence metric.

**Results.** The results, illustrated in Figure 4, verify that the error diminishes in direct proportion to the inverse of the number of points utilized in calculating the adversarial hypervolume. Furthermore, once the point count surpasses 10, the error becomes negligible, suggesting that our approximation achieves sufficient precision.

TABLE IV  
ADVERSARIAL HYPERVOLUME, ALONG WITH ADVERSARIAL ACCURACY OF DEFENSIVE MODELS UNDER MODIFIED AUTOATTACK [14] ON THE CIFAR-10 DATASET. THE CONFIDENCE LOSS IF THE MARGINAL LOSS MENTIONED IN EQUATION (4) [14].

Model	Defense	$\ell_2$ Attack		$\ell_\infty$ Attack	
		Acc. (Std./Adv.)	AH (mean <sub>std</sub> )	Acc. (Std./Adv.)	AH (mean <sub>std</sub> )
WideResNet-28-10	None	94.78/02.58	0.2127 <sub>0.2191</sub>	94.78/01.65	0.0912 <sub>0.1905</sub>
ResNet-18	Madry <i>et al.</i> (2018) [1]	80.75/72.79	0.5726 <sub>0.4019</sub>	82.59/19.24	0.3658 <sub>0.3553</sub>
WideResNet-28-10	Wang <i>et al.</i> (2023) [40]	95.16/86.66	0.6171 <sub>0.2900</sub>	92.44/72.35	0.4286 <sub>0.2970</sub>
WideResNet-28-10	Rebuffi <i>et al.</i> (2021) [47]	91.79/83.31	0.5814 <sub>0.3296</sub>	87.33/67.91	0.3976 <sub>0.3233</sub>
WideResNet-70-16	Rebuffi <i>et al.</i> (2021) [47]	92.41/84.80	0.6206 <sub>0.3310</sub>	88.54/70.97	0.4437 <sub>0.3351</sub>
WideResNet-70-16	Rebuffi <i>et al.</i> (2021) [47] (w/ data)	95.74/85.18	0.7037 <sub>0.2990</sub>	92.23/71.84	0.5188 <sub>0.3326</sub>
ResNet-18	Sehwag <i>et al.</i> (2022) [48]	89.76/80.05	0.6460 <sub>0.3754</sub>	84.59/64.23	0.4395 <sub>0.3649</sub>
WideResNet-34-10	Sehwag <i>et al.</i> (2022) [48]	90.93/77.24	0.6772 <sub>0.3717</sub>	86.68/60.27	0.5075 <sub>0.3884</sub>
ResNet-18	Rade <i>et al.</i> (2022) [49]	90.57/81.27	0.5951 <sub>0.3350</sub>	86.86/64.81	0.3719 <sub>0.3127</sub>
ResNet-50	Augustin <i>et al.</i> (2020) [44]	91.08/78.81	0.5552 <sub>0.3626</sub>	-	-
WideResNet-34-10	Augustin <i>et al.</i> (2020) [44]	92.23/81.03	0.5746 <sub>0.3584</sub>	-	-
WideResNet-34-10	Huang <i>et al.</i> (2021) [50]	-	-	90.56/67.80	0.5078 <sub>0.3511</sub>
WideResNet-34-10	Huang <i>et al.</i> (2021) [50] (EMA)	-	-	91.23/68.54	0.5051 <sub>0.3520</sub>
WideResNet-28-10	<b>Ours</b>	91.43/88.57	0.5762 <sub>0.3165</sub>	88.87/63.62	0.4173 <sub>0.2270</sub>

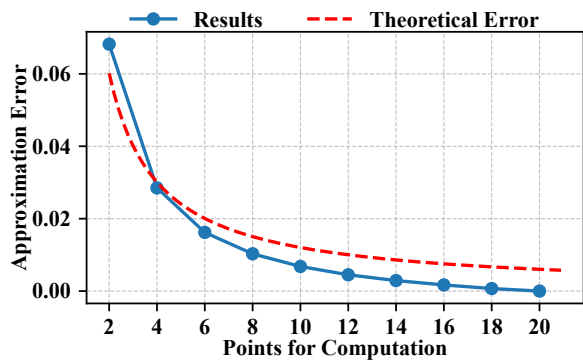


Fig. 4. An illustration of computed and theoretical error between the adversarial hypervolume and the true integral of the confidence loss (Adversarial hypervolume approximated using  $N = 20$  points as a proxy). The computed values are represented by the blue line, while the theoretical error function is depicted with a red dashed line.

### F. Additional Results with Marginal Loss

In our paper, we use two loss functions for computing the adversarial hypervolume. The result using the normalized confidence score is shown in the previous sections. Here we show the results using the marginal loss.

## VI. DISCUSSION

### A. Normalized Cross Entropy Loss

In this section, we present a theorem that elucidates an example’s misclassification occasioned by negative normalized cross entropy loss values.

**Theorem 3.** *A negative normalized cross entropy loss implies the inevitable misclassification of the perturbed input.*

*Proof.* Given a classifier ( $f$ ) providing a probability distribution over ( $m$ ) classes and an original example ( $x$ ) with

perturbation ( $\delta$ ), it holds that:

$$\forall j \in \{1, \dots, m\}, 0 \leq f_j(x + \delta) \leq 1 \text{ and } \sum_i^m f_i(x + \delta) = 1. \quad (13)$$

If the classifier’s normalized confidence loss drops below zero, as indicated by:

$$\frac{\log m + \log f_y(x + \delta)}{\log m} < 0, \quad (14)$$

$$f_y(x + \delta) < \frac{1}{m},$$

$$\sum_{j \neq y} f_j(x + \delta) > \frac{m-1}{m},$$

then we infer that:

$$\exists t \neq y, f_t(x + \delta) > \frac{1}{m} > f_y(x + \delta). \quad (15)$$

This necessitates the conclusion that the perturbed input ( $x + \delta$ ) is incorrectly classified as class ( $t$ ).  $\square$

### B. Why Adversarial Hypervolume?

The adoption of adversarial hypervolume as a metric to evaluate the robustness of neural network models is justified by several compelling reasons:

- **Multiobjective Nature.** Since attacking a neural network model constitutes a multiobjective optimization problem, a metric that encapsulates the trade-offs between distance and confidence is essential. Adversarial hypervolume aptly fulfills this requirement.
- **Limitations of Current Metrics.** Although adversarial accuracy offers a straightforward assessment of robustness, it falls short in guiding researchers to pinpoint areas of improvement and to differentiate between models with similar adversarial accuracy scores. Adversarial sparsity and probability metrics attempt to capture the robustness

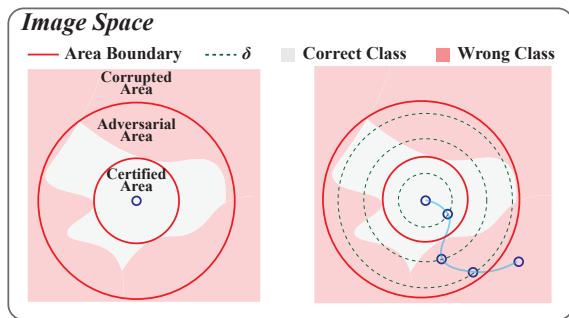


Fig. 5. An illustration of three regions and the adversarial frontier in the image sample space. The blue curve denotes the adversarial frontier.

from different perspectives but are constrained to analyzing the misclassified sample space. In contrast, adversarial hypervolume emphasizes the correctly classified sample space.

- **A Natural Interpretation.** Beyond these benefits, our metric provides an intuitive interpretation since it represents the sample set with worst confidence scores across the perturbation levels. Our further research on this adversarial frontier is planned to yield insights for the development of more robust models.

### C. Intuition of the Proposed Metric

This subsection introduces the conceptual foundation underlying the proposed metric. For visual representation of the image sample space, the misclassification area is highlighted in red, while a grey zone encircles the correctly classified examples adjacent to the original sample, as illustrated in Fig. 5. The space is segmented into three distinct regions relative to the  $\ell_2$ -norm: the certified region, the adversarial region, and the corrupted region.

- **Certified Region.** Within this domain, demarcated by the established perturbation limit, all samples are guaranteed to be classified accurately. The range of this particular area partially reflects the robustness of the model.
- **Adversarial Region.** This zone contains a mix of correctly and incorrectly classified samples. The proportion of misclassified instances within this region correlates with the level of adversarial sparsity [18].
- **Corrupted Region.** Samples in this domain are invariably misclassified.

Fig. 5 presents a schematic depiction of the three regions within the image sample space, featuring the adversarial frontier as a blue curve. This frontier delineates samples with minimum confidence scores at specific perturbation intensities.

Upon projecting the aforementioned space onto a distance-confidence plane, Fig. 6 emerges, with the shaded portion exemplifying the image space across the three delineated areas. Our metric, termed adversarial hypervolume, calculates an average for the certified area while also accounting for the confidence score, thereby providing enriched information.

### D. Limitation of the Proposed Metric

We consider the trade off between the confidence and the distance, which is a major advantage. However, we do not

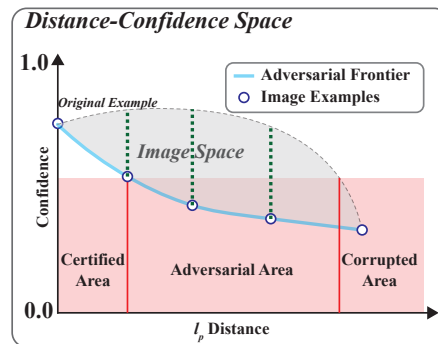


Fig. 6. An illustration of the projection of the image space onto the distance-confidence space.

separately show the clean space and the adversarial space, which can cause inaccurate measurement of the robustness. We will address this issue in future work.

## VII. CONCLUSION

We proposed the adversarial hypervolume metric, offering a comprehensive evaluation of deep learning model robustness across varying perturbation intensities. Our findings indicate that this metric surpasses traditional adversarial accuracy in capturing incremental robustness improvements and provides a deeper understanding of model resilience. The adversarial hypervolume facilitates the development of robust deep learning systems and sets a new standard for robustness assessment in the face of adversarial threats.

## REFERENCES

- [1] A. Madry, A. Makelov, L. Schmidt, D. Tsipras, and A. Vladu, “Towards deep learning models resistant to adversarial attacks,” in *6th International Conference on Learning Representations, (ICLR)*. OpenReview.net, 2018.
- [2] M. Ren, W. Zeng, B. Yang, and R. Urtasun, “Learning to reweight examples for robust deep learning,” in *Proceedings of the 35th International Conference on Machine Learning, (ICML)*, ser. Proceedings of Machine Learning Research. PMLR, 2018.
- [3] H. Salman, J. Li, I. P. Razenshteyn, P. Zhang, H. Zhang, S. Bubeck, and G. Yang, “Provably robust deep learning via adversarially trained smoothed classifiers,” in *Advances in Neural Information Processing Systems 32: Annual Conference on Neural Information Processing Systems 2019, (NeurIPS)*, 2019.
- [4] Y. Dong, Z. Deng, T. Pang, J. Zhu, and H. Su, “Adversarial distributional training for robust deep learning,” in *Advances in Neural Information Processing Systems 33: Annual Conference on Neural Information Processing Systems 2020, (NeurIPS)*, 2020.
- [5] K. Sadeghi, A. Banerjee, and S. K. S. Gupta, “A system-driven taxonomy of attacks and defenses in adversarial machine learning,” *IEEE Trans. Emerg. Top. Comput. Intell.*, vol. 4, no. 4, pp. 450–467, 2020. [Online]. Available: <https://doi.org/10.1109/TETCI.2020.2968933>
- [6] C. Szegedy, W. Zaremba, I. Sutskever, J. Bruna, D. Erhan, I. J. Goodfellow, and R. Fergus, “Intriguing properties of neural networks,” in *2nd International Conference on Learning Representations (ICLR)*, 2014.
- [7] I. J. Goodfellow, J. Shlens, and C. Szegedy, “Explaining and harnessing adversarial examples,” in *3rd International Conference on Learning Representations, (ICLR)*, 2015.
- [8] A. Kurakin, I. J. Goodfellow, and S. Bengio, “Adversarial examples in the physical world,” in *5th International Conference on Learning Representations, ICLR*. OpenReview.net, 2017.
- [9] Y. Dong, H. Su, B. Wu, Z. Li, W. Liu, T. Zhang, and J. Zhu, “Efficient decision-based black-box adversarial attacks on face recognition,” in *IEEE Conference on Computer Vision and Pattern Recognition, CVPR*. Computer Vision Foundation / IEEE, 2019.

- [10] Y. Cao, C. Xiao, B. Cyr, Y. Zhou, W. Park, S. Rampazzi, Q. A. Chen, K. Fu, and Z. M. Mao, "Adversarial sensor attack on lidar-based perception in autonomous driving," in *Proceedings of the 2019 ACM SIGSAC Conference on Computer and Communications Security, (CCS)*. ACM, 2019.
- [11] N. Carlini and D. A. Wagner, "Towards evaluating the robustness of neural networks," in *2017 IEEE Symposium on Security and Privacy, SP*. IEEE Computer Society, 2017.
- [12] A. Athalye, N. Carlini, and D. A. Wagner, "Obfuscated gradients give a false sense of security: Circumventing defenses to adversarial examples," in *Proceedings of the 35th International Conference on Machine Learning, ICML*, ser. Proceedings of Machine Learning Research. PMLR, 2018.
- [13] S. Moosavi-Dezfooli, A. Fawzi, and P. Frossard, "Deepfool: A simple and accurate method to fool deep neural networks," in *2016 IEEE Conference on Computer Vision and Pattern Recognition, (CVPR)*. IEEE Computer Society, 2016.
- [14] F. Croce and M. Hein, "Reliable evaluation of adversarial robustness with an ensemble of diverse parameter-free attacks," in *Proceedings of the 37th International Conference on Machine Learning, (ICML)*, ser. Proceedings of Machine Learning Research. PMLR, 2020.
- [15] M. Andriushchenko, F. Croce, N. Flammarion, and M. Hein, "Square attack: A query-efficient black-box adversarial attack via random search," in *Computer Vision - ECCV 2020 - 16th European Conference, Glasgow, UK*, ser. Lecture Notes in Computer Science. Springer, 2020.
- [16] F. Croce, M. Andriushchenko, V. Schwag, E. Debenedetti, N. Flammarion, M. Chiang, P. Mittal, and M. Hein, "Robustbench: A standardized adversarial robustness benchmark," in *Proceedings of the Neural Information Processing Systems Track on Datasets and Benchmarks 1, NeurIPS Datasets and Benchmarks 2021*, 2021.
- [17] A. Robey, L. F. O. Chamon, G. J. Pappas, and H. Hassani, "Probabilistically robust learning: Balancing average and worst-case performance," in *International Conference on Machine Learning, (ICML)*, ser. Proceedings of Machine Learning Research. PMLR, 2022.
- [18] R. Olivier and B. Raj, "How many perturbations break this model? evaluating robustness beyond adversarial accuracy," in *International Conference on Machine Learning, (ICML)*, ser. Proceedings of Machine Learning Research. PMLR, 2023.
- [19] W. Xu, D. Evans, and Y. Qi, "Feature squeezing: Detecting adversarial examples in deep neural networks," in *25th Annual Network and Distributed System Security Symposium, NDSS*. The Internet Society, 2018.
- [20] J. Bader and E. Zitzler, "Hype: An algorithm for fast hypervolume-based many-objective optimization," *Evol. Comput.*, 2011.
- [21] K. Deb, K. Sindhya, and J. Hakanen, "Multi-objective optimization," in *Decision sciences*. CRC Press, 2016, pp. 161–200.
- [22] K. Deb, S. Agrawal, A. Pratap, and T. Meyarivan, "A fast and elitist multiobjective genetic algorithm: NSGA-II," *IEEE Trans. Evol. Comput.*, 2002.
- [23] Q. Zhang and H. Li, "MOEA/D: A multiobjective evolutionary algorithm based on decomposition," *IEEE Trans. Evol. Comput.*, 2007.
- [24] N. Akhtar and A. S. Mian, "Threat of adversarial attacks on deep learning in computer vision: A survey," *IEEE Access*, 2018.
- [25] G. R. Machado, E. Silva, and R. R. Goldschmidt, "Adversarial machine learning in image classification: A survey toward the defender's perspective," *ACM Comput. Surv.*, 2023.
- [26] B. Li, P. Qi, B. Liu, S. Di, J. Liu, J. Pei, J. Yi, and B. Zhou, "Trustworthy AI: from principles to practices," *ACM Comput. Surv.*, 2023.
- [27] S. Bhambri, S. Muku, A. Tulasi, and A. B. Buduru, "A survey of black-box adversarial attacks on computer vision models," *arXiv preprint arXiv:1912.01667*, 2019.
- [28] Z. Li, H. Cheng, X. Cai, J. Zhao, and Q. Zhang, "SA-ES: subspace activation evolution strategy for black-box adversarial attacks," *IEEE Trans. Emerg. Top. Comput. Intell.*, vol. 7, no. 3, pp. 780–790, 2023. [Online]. Available: <https://doi.org/10.1109/TETCI.2022.3214627>
- [29] H. Li, X. Xu, X. Zhang, S. Yang, and B. Li, "QEBA: query-efficient boundary-based blackbox attack," *CoRR*, vol. abs/2005.14137, 2020. [Online]. Available: <https://arxiv.org/abs/2005.14137>
- [30] Q. Fu, Y. Dong, H. Su, J. Zhu, and C. Zhang, "Autoda: Automated decision-based iterative adversarial attacks," in *31st USENIX Security Symposium, USENIX Security 2022, Boston, MA, USA, August 10-12, 2022*, K. R. B. Butler and K. Thomas, Eds. USENIX Association, 2022, pp. 3557–3574. [Online]. Available: <https://www.usenix.org/conference/usenixsecurity22/presentation/fu-qi>
- [31] P. Guo, F. Liu, X. Lin, Q. Zhao, and Q. Zhang, "L-autoda: Leveraging large language models for automated decision-based adversarial attacks," *CoRR*, vol. abs/2401.15335, 2024. [Online]. Available: <https://doi.org/10.48550/arXiv.2401.15335>
- [32] H. Zanddizari, B. Zeinali, and J. M. Chang, "Generating black-box adversarial examples in sparse domain," *IEEE Trans. Emerg. Top. Comput. Intell.*, vol. 6, no. 4, pp. 795–804, 2022. [Online]. Available: <https://doi.org/10.1109/TETCI.2021.3122467>
- [33] T. Bai, J. Luo, J. Zhao, B. Wen, and Q. Wang, "Recent advances in adversarial training for adversarial robustness," in *Proceedings of the Thirtieth International Joint Conference on Artificial Intelligence, (IJCAI)*. ijcai.org, 2021.
- [34] C. Guo, M. Rana, M. Cissé, and L. van der Maaten, "Countering adversarial images using input transformations," in *6th International Conference on Learning Representations, (ICLR)*. OpenReview.net, 2018.
- [35] P. Guo, Z. Yang, X. Lin, Q. Zhao, and Q. Zhang, "Puriddefense: Randomized local implicit adversarial purification for defending black-box query-based attacks," *CoRR*, 2024.
- [36] N. Carlini, F. Tramèr, K. D. Dvijotham, L. Rice, M. Sun, and J. Z. Kolter, "(certified!) adversarial robustness for free!" in *The Eleventh International Conference on Learning Representations, (ICLR)*. OpenReview.net, 2023.
- [37] S. Ma, Y. Liu, G. Tao, W. Lee, and X. Zhang, "NIC: detecting adversarial samples with neural network invariant checking," in *26th Annual Network and Distributed System Security Symposium, (NDSS)*. The Internet Society, 2019.
- [38] H. Li, S. Shan, E. Wenger, J. Zhang, H. Zheng, and B. Y. Zhao, "Blacklight: Scalable defense for neural networks against query-based black-box attacks," in *31st USENIX Security Symposium, USENIX Security 2022*. USENIX Association, 2022.
- [39] H. Zhang, Y. Yu, J. Jiao, E. P. Xing, L. E. Ghaoui, and M. I. Jordan, "Theoretically principled trade-off between robustness and accuracy," in *Proceedings of the 36th International Conference on Machine Learning, (ICML)*, ser. Proceedings of Machine Learning Research. PMLR, 2019.
- [40] Z. Wang, T. Pang, C. Du, M. Lin, W. Liu, and S. Yan, "Better diffusion models further improve adversarial training," in *International Conference on Machine Learning, (ICML)*, ser. Proceedings of Machine Learning Research. PMLR, 2023.
- [41] S. Goyal, C. Qin, J. Uesato, T. A. Mann, and P. Kohli, "Uncovering the limits of adversarial training against norm-bounded adversarial examples," *CoRR*, 2020.
- [42] A. Krizhevsky, "Learning Multiple Layers of Features from Tiny Images," Univ. Toronto, Technical Report, 2009.
- [43] R. Rade and S.-M. Moosavi-Dezfooli, "Helper-based adversarial training: Reducing excessive margin to achieve a better accuracy vs. robustness trade-off," in *ICML 2021 Workshop on Adversarial Machine Learning, 2021*. [Online]. Available: <https://openreview.net/forum?id=BuD2LmNaU3a>
- [44] M. Augustin, A. Meinke, and M. Hein, "Adversarial robustness on in- and out-distribution improves explainability," in *Computer Vision - ECCV 2020 - 16th European Conference*, ser. Lecture Notes in Computer Science. Springer, 2020.
- [45] D. Wu, S. Xia, and Y. Wang, "Adversarial weight perturbation helps robust generalization," in *Advances in Neural Information Processing Systems 33: Annual Conference on Neural Information Processing Systems 2020, (NeurIPS)*, 2020.
- [46] S. Addepalli, S. Jain, and V. B. R., "Efficient and effective augmentation strategy for adversarial training," in *Advances in Neural Information Processing Systems 35: Annual Conference on Neural Information Processing Systems 2022, (NeurIPS)*, 2022.
- [47] S. Rebuffi, S. Goyal, D. A. Calian, F. Stimberg, O. Wiles, and T. A. Mann, "Fixing data augmentation to improve adversarial robustness," *CoRR*, 2021.
- [48] V. Schwag, S. Mahloujifar, T. Handina, S. Dai, C. Xiang, M. Chiang, and P. Mittal, "Robust learning meets generative models: Can proxy distributions improve adversarial robustness?" in *The Tenth International Conference on Learning Representations, (ICLR)*. OpenReview.net, 2022.
- [49] R. Rade and S. Moosavi-Dezfooli, "Reducing excessive margin to achieve a better accuracy vs. robustness trade-off," in *The Tenth International Conference on Learning Representations, (ICLR)*. OpenReview.net, 2022.
- [50] H. Huang, Y. Wang, S. M. Erfani, Q. Gu, J. Bailey, and X. Ma, "Exploring architectural ingredients of adversarially robust deep neural networks," in *Advances in Neural Information Processing Systems 34: Annual Conference on Neural Information Processing Systems 2021, (NeurIPS)*, 2021.

- [51] S. Diamond and S. Boyd, “CVXPY: A Python-embedded modeling language for convex optimization,” *Journal of Machine Learning Research*, vol. 17, no. 83, pp. 1–5, 2016.